

The Effect of K-Doping on Activation in Co-Free Li-Rich Cathodes

 Trent Seaby,^{*,[a]} Tongen Lin,^[a] Xia Huang,^[a] Ardeshir Baktash,^[a] and Lianzhou Wang^{*,[a]}

The activation mechanism of Li-rich cathode has been discussed for many years, yet there is still debate on different theories. Potassium doping can assist the investigation on activation mechanism through its unique function in terms of blocking TM migration during activation. K-doping works by occupying Li sites even after Li has been extracted, increasing stability by blocking transition metals from migrating into these sites, which can help us distinguish the pathway of activation. We use in-situ XRD to show that K-doping significantly lowers the rate of transition metal migration during initial charging, and

that this is correlated with less activation extent. However, the ex-situ XAS results show that anionic redox is more reversible in the K-doped material. These results cannot be easily explained by existing theories alone; therefore, we propose that K-doping hinders TM migration during activation and therefore favours a Reductive Coupling Mechanism over a dynamic TM migration mechanism. These findings have significant practical and theoretical implications for the development of Lithium-Rich cathodes.

Introduction

Lithium-Rich Cathodes (LRCs) are one of the most promising future technologies for Lithium-Ion Batteries (LIBs). They have exceptional capacity (> 250 mAh/g), however their poor stability caused by activation has limited their practical applications.^[1] The activation mechanism of LRCs is still uncertain, and the dynamics of TM migration are crucial to our current understanding.^[2–4] There are three main mechanisms that are used to explain activation; the static Reductive Coupling Mechanism (RCM),^[4] the dynamic inter-layer TM migration mechanism,^[2] and the intra-layer TM migration controlled trapped O₂ mechanism.^[3] The mechanism of anionic redox stabilisation is subtly different in each one. In the RCM the stability is determined entirely by the electronic structure of the crystal, specifically the relative energy of TM–O and O–O molecular orbitals. In the dynamic TM migration mechanism, TM migration from the TM layer into the Li layer is required to stabilise oxygen redox. Finally, the trapped O₂ mechanism proposes that oxygen redox proceeds all the way to molecular O₂, however these molecules are trapped in ‘nanovoids’ created by intra-layer TM migration.

K⁺ has a very large size relative to Li⁺, meaning it remains in the Li layer throughout activation and blocks TM migration. Additionally, its outer most orbital is a 2s orbital, meaning that it does not bond with the TM 3d orbitals. The electronic structure is therefore unaltered while the dynamics of TM migration are significantly changed. Potassium doping has been explored as a potential stabilising dopant in LRCs, and it can inhibit long term structural decay via a ‘pillar-ion’ effect.^[5] However, it is overlooked that such an effect not only theoretically reduces TM migration during long-term cycling, but also reduces TM migration during activation,^[6] which can assist the understanding of activation mechanism. After Li⁺ is extracted, the spinel phase is thermodynamically favoured over the layered phase and there is therefore a driving force encouraging transition.^[7] Stability is therefore only maintained through kinetic limitations. The logic underlying all pillar-ion doping is that they physically block TMs migrating into the Li layer and causing the layered-to-spinel transition. Electrochemical tests consistently show a reduction in spinel phase formation in pillar-ion doped materials compared to undoped materials,^[5,6,8–14] with Zhao et al.^[10] demonstrated that the much larger size of the K⁺ ions results in lower diffusivity (compared to Li⁺) and therefore K⁺ remaining in the Li layer during discharge. The main barrier to migration is the activation energy of the tetrahedral site hop, which is determined by the size of ion and the charge of the ion.^[15] The much larger ionic size of K⁺ compared to Li⁺ means that the diffusivity of K⁺ is reduced to the point where it is effectively inert.^[9] Additionally, Ceder et al.^[7] showed that the TM’s migration energy into the Li layer significantly increased from a completely delithiated to a partially lithiated structure. This was largely due to cation-cation repulsion, which is similar for both K⁺ and Li⁺ given their identical charges. K-doping therefore blocks TM migration into the Li layer over dozens of cycles, and it is reasonable to assume that it will also have the same effect during activation.

[a] T. Seaby, T. Lin, X. Huang, A. Baktash, L. Wang
 Nanomaterial Centre, School of Chemical Engineering, The University of
 Queensland, St. Lucia, QLD 4072,
 Australia
 E-mail: t.seaby@uq.edu.au
 l.wang@uq.edu.au

Supporting information for this article is available on the WWW under
<https://doi.org/10.1002/asia.202400185>

© 2025 The Author(s). Chemistry - An Asian Journal published by Wiley-VCH
 GmbH. This is an open access article under the terms of the Creative
 Commons Attribution Non-Commercial License, which permits use, dis-
 tribution and reproduction in any medium, provided the original work is
 properly cited and is not used for commercial purposes.

One might expect the much larger size of K^+ compared to Li^+ to significantly increase the c -parameter spacing, and this has been observed.^[13,16] However, the additional strain caused by K^+ can result in the overall c -parameter being decreased.^[5,17] XRD results are therefore not sufficient to establish K^+ 's occupation of Li sites. Additionally, the electronic similarity between Li^+ and K^+ mean it is very difficult to distinguish between the two using techniques such as SEM and TEM. For this reason, the precise site of K^+ doping has not been definitely shown. However, the assumption that it occupies the Li^+ sites is reasonable based on the electronic similarity between the two ions and the overall behaviour of the K-doped material.^[5,6,16]

This paper exploits the pillar ion doping effect to investigate the activation mechanism. K-doping prevents inter-layer migration, while theoretically having relatively little effect on intra-layer migration. If the reversible TM migration theory is correct, K-doping will therefore have a significant impact on activation. It will decrease the total number of TM ions that migrate into the Li layer, thereby decreasing the total amount of activation. However, the effect will be much less if the trapped O_2 theory is correct. Although K-doping has a significant effect on inter-layer TM migration by physically blocking the migration pathway, it does not have the same effect on intra-layer migration. The extra susceptibility to TM migration of Co-free materials exacerbates the differences between the two theories, magnifying the effect of K-doping.

In-situ XRD, ex-situ XAS, XPS, DFT simulations, and Raman spectroscopy, are used to characterise the material and check if the transformations conform with theoretical predictions. We find that the in-situ XRD results show that the rate of structural transformation is significantly slower in the K-doped material. There was also a significant difference observed in the electronic structural change, with Ni L-edge results showing that Ni is oxidised in the K-doped sample during activation but reduced in the pristine sample. Simultaneously, the O K-edge results show clear evidence of oxygen loss in the pristine sample that is not present in the K-doped sample. Additionally, a characteristic peak from the Reductive Coupling Mechanism (RCM) for anionic redox appears in K-doped sample but not in the pristine sample. The DFT and XPS results, meanwhile, show that K-doping has a negligible impact on the electronic structure of the crystal.

All these results suggest that the most common activation mechanisms interact with each other in a feedback loop. Oxygen vacancies generated during the initial activation trigger TM migration, which in turn generates more activation and oxygen loss according to the mechanism described by Gent et al.^[2] The activation during the initial stage is similar for both samples, however K-doping limits the additional activation generated in the TM migration stage. This explains why K-doping has lower overall capacity during the first cycle and yet has more evidence of anionic redox from the RCM. Importantly, this implies that both mechanisms are of critical importance to activation, and that the interaction between the two mechanisms is just as important as either mechanism alone. This has

important ramifications, both for the fundamental activation mechanism of LRCs and for the practical design of future cells.

Experimental Methodology

Cathode Synthesis

The sol-gel method was used, with stoichiometric amounts of Lithium Acetate (CH_3COOLi), Manganese(II) Acetate dihydrate ($Mn(CH_3CO_2)_2 \cdot H_2O$), Nickel(II) Acetate tetrahydrate ($Ni(CH_3CO_2)_2 \cdot 4H_2O$) added to distilled water to make a 1 M solution. The nominal composition was $Li_{1.2}Mn_{0.54}Ni_{0.26}O_2$. For the K-doped sample, Potassium Acetate (CH_3COOK) was added alongside the other precursors in a molar ratio of 1:27 Potassium Acetate:Manganese. The number of moles of Lithium Acetate was reduced by the same number of moles of Potassium Acetate added, to compensate for the K substitution. The stoichiometric mass of Lithium Acetate was then multiplied by 1.05 (by weight) to account for Li decomposition during high-temperature calcination. Acrylic acid was added to this solution as a chelating agent in a 1:1.4 metal:acid ratio. The solution was then mixed at 70 °C until a gel was formed. This gel was pre-calcined to remove organic compounds using a heating protocol of 200 °C for 3 hrs, 350 °C for 3 hrs, and finally 450 °C for 3 hrs. The resultant powder was then calcined under air at 900 °C for 10 hrs.

Battery Assembly

The synthesized cathode materials were combined with a pre-mixed 40:1:1 NMP:PvDF:Carbon Black slurry in a 1:5 ratio and mixed overnight to create and 80:10:10 active material:PvDF:Carbon Black final cathode (all by weight). The slurry was then coated to a thickness of 250 μm on a carbon-coated Al foil substrate. The substrate was then dried for 12 hrs at 110 °C in a vacuum oven before being calendered on an MTI MSK-HRP-MR100A machine. 13 mm diameter circular cathodes were then punched out of the foil.

Coin cells were constructed in an Ar glovebox. Li foil, 35 μL of 1 M $LiPF_6$ in 1:1:1 EC:DEC:DMC, and Celgard 2325 polymer comprise the anode, separator, and electrolyte respectively. The cells were sealed using an MTI MSK-160E electric crimping machine. The batteries were then left for at least 12 hrs to ensure proper penetration of electrolyte into the cathode.

Electrochemical Testing

Low-rate testing was a galvanostatic program between 2.0–4.8 V at 25 mAh/g of active material (~0.1 C) for 100 cycles. These tests were conducted on a LAND CT3001A battery testing machine.

In-Situ XRD

Different electrochemical cells were required for the in-situ synchrotron experiments. 0.6 mm diameter holes were cut into the centre of the anode and cathode casing to allow the beam to penetrate the cell. These were sealed on both the inside and outside with Kapton Tape. AL foil rings were then stuck to the outside of both cases to improve conductivity. Cu foil was used as a current collector for the anode while Al was used for the cathode.

Several different techniques during cell construction were used to optimize the performance of the cell in-situ. The cell is compromised to allow in-situ measurements, and so optimising perform-

ance is essential. Cells were left to rest for 10 hrs before testing to ensure that there was enough time for the electrolyte to soak into the cathode but not enough time for the performance to degrade. Any dendrites or burrs left on the cases from the hole-punching process are potentially catastrophic for cell performance, as they can pierce the Kapton tapes, and so all cases were checked and only those without these defects were used. It was also noted that the 'smoothness' of the fit between the metal foils and the cathode/anode case had a substantial impact on performance. Not only did rough fits appear to reduce conductivity, they also appeared to increase the failure rate of cells. Furthermore, carbon paper was used as the substrate for the cathode rather than Al foil to avoid overlap between the 45° and 65° Al peaks and the (101) and (110)/(113) R3m reflections in the sample. Finally, performance can become electrolyte limited as soon as the first cycle discharge, and so the amount of electrolyte was doubled from 35 μL to 70 μL . All of these small refinements are necessary for the electrochemical performance to be reliable and to a level where phenomena like activation can be observed.

SEM and EDS

SEM images and EDS maps were taken on a JEOL 7800 machine. To ensure high-quality images, the surface of the samples was cleaned using an Evactron vacuum plasma cleaner for 5 minutes. Samples were then carbon coated with a Quantum Design Q150T ES Plus to a thickness of ~ 3 nm. Images were collected at a 10 keV working voltage with a probe current of 13.

XPS and Raman

XPS was conducted on a Kratos Axis Supra Plus XPS machine. Raman spectroscopy was conducted on Renishaw Raman microscope at a laser wavelength of 785 nm.

Computation Methodology

In this study, all calculations were performed using Density Functional Theory (DFT) within the Vienna Ab Initio Package (VASP).^[18] The exchange-correlation effect was accounted for using the Perdew-Burke-Ernzehof (PBE) functional through generalized gradient approximation (GGA) method.^[19] To consider Van der Waals interactions, a D3-BJ dispersion correction was employed.^[20,21] The core and valence electrons were described using the projector augmented-wave (PAW) method, with an energy cutoff of 520 eV and a force tolerance of 0.01 eV \AA^{-1} . A supercell with $2 \times 1 \times 2$ unitcell of Li_2MnO_3 (96 atoms) with a C12/m1 crystallographic space group [space group 12] considered for the DFT calculations.

Results and Discussion

XPS results (Figure 1) demonstrate that K has been successfully doped into the lattice. The peaks at $\sim 297 \text{ eV}$ and $\sim 294 \text{ eV}$ can be assigned to the K $2p_{1/2}$ and K $2p_{3/2}$ orbital binding energies,^[5,22] with additional small differences in the adventitious carbon peak (Figure 1a).^[23] The two transition metal peaks, Ni 2p (Figure 1b) and Mn 2p (Figure 1c), show only very minor differences between the two samples. This is to be expected, as K^+ has no available orbitals that can easily hybridise with TM $3d$ orbitals. Additionally, the O 1s binding energy shows a similarly negligible difference between the two samples (Figure 1d). Although K^+ is larger than Li^+ , the additional steric effect is not enough to significantly alter the electronic structure of the oxygen ions. The successful incorporation of K into the material therefore does not meaningfully alter the electronic structure.

EDS results confirm the incorporation of K into the material for the K-doped sample. Figure 2 shows the EDS results for the Pristine (Figure 2a) and the K-doped (Figure 2b) sample along

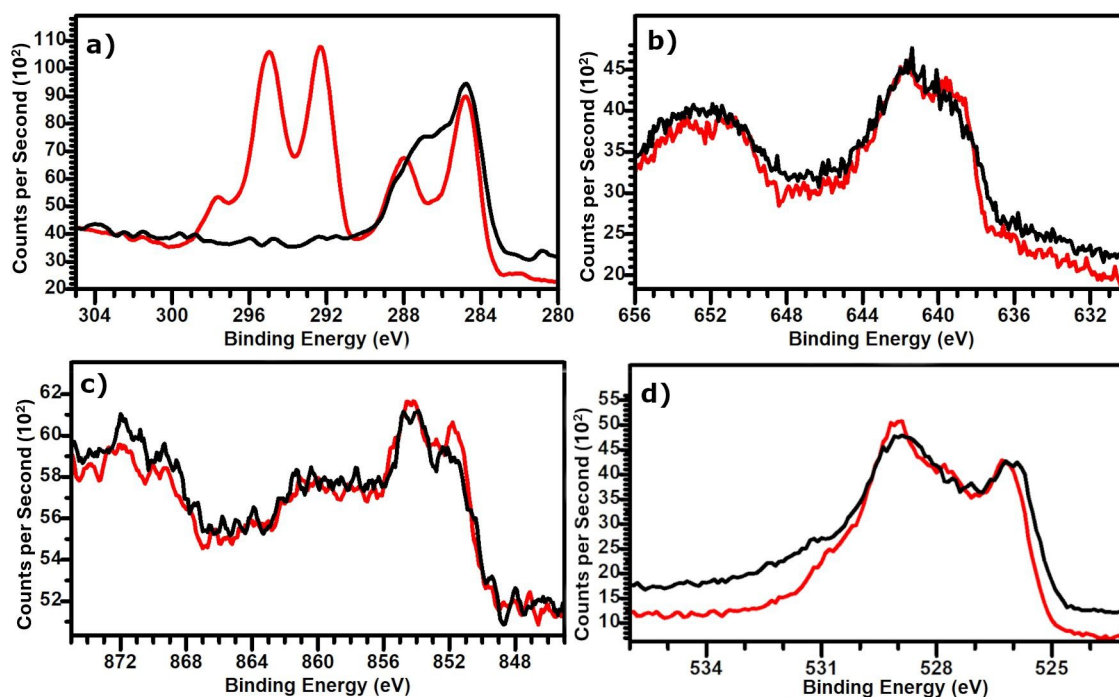


Figure 1. XPS results for the a) K 2p and C 1s, b) Mn 2p, c) Ni 2p, and d) O 1s regions for the Pristine and K-doped samples.

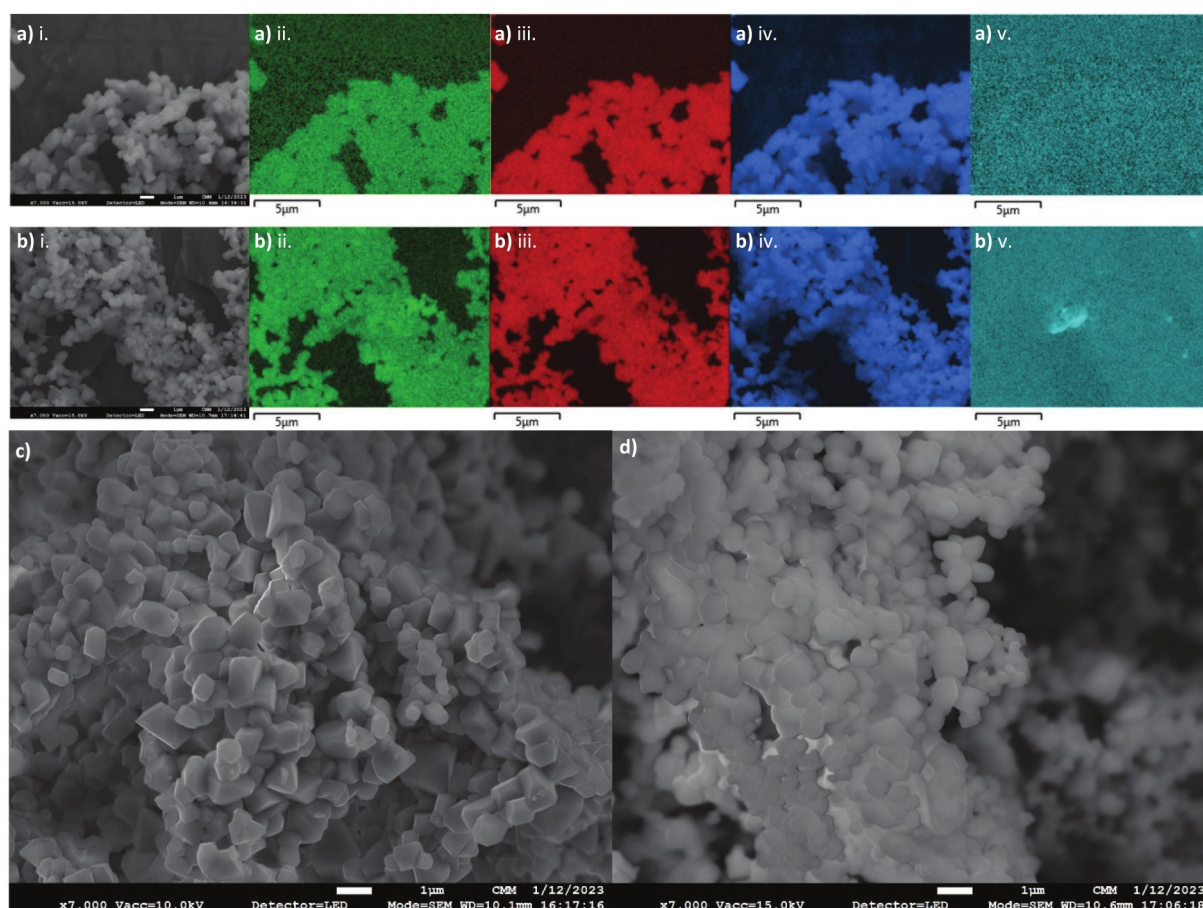


Figure 2. SEM and EDS images for the a) Pristine and b) K-doped material, with the i. SEM image, ii. Ni, iii. Mn, iv. O, and v. K. High-definition SEM images for the c) Pristine and d) K-doped samples are also shown.

with an SEM image. Both samples display the expected, even distribution of O, Ni, and Mn throughout the sample, with the Pristine sample also displaying no evidence of K. There is a visible K signal in the K-doped sample, with the much smaller intensity commensurate with K's much lower concentration. ICP results suggest that the concentration of K is relatively high, ~6.7 wt% in the doped material compared to ~0.1 wt% in the pristine material (Supplementary Table S1). Finally, the SEM images shows no clear difference in particle size or morphology between the two samples. Differences in electrochemical behaviour are therefore unlikely to be explained by macro-scale physical parameters like surface-area-to-volume ratio or diffusion path length. The EDS results therefore show the compositional differences and morphological similarities between the samples.

The electrochemical performance results shown in Figure 3 indicate that K-doping is having the expected effect on capacity. K-doping lowers the energy but increases the stability (Figure 3a), consistent with K^+ occupying Li^+ sites and blocking inter-layer TM migration (Capacity results reported in Supplementary Figure 1). Rather than activation occurring over 1 cycle, the Co-free materials activate over 10–15 cycles. The capacity of the K-doped material is still increasing after 50 cycles, however,

indicating that K-doping significantly slows the rate of activation.

Figure 3b shows that the mid-point voltage of the K-doped material is substantially higher than the pristine sample. This is beneficial from an energy density perspective, but it also hints at a fundamental difference in activation and electrochemical behaviour between the two samples. The dQ/dV graphs reveal more information about the differences in voltage. Each peak on a dQ/dV graph corresponds to a redox reaction. $Mn^{4+/3+}$ reduction, the redox reaction created by activation, is reflected in the 3.0 V–3.5 V peak. The $Ni^{2+/4+}$ redox is associated with the region between 3.5 V–4.0 V, while the height of the peak at 4.5 V corresponds to the length of the activation plateau. The peak between 3.0–3.5 V is suppressed in the K-doped sample during the first cycle, meaning there is less $Mn^{4+/3+}$ reduction and that the activation has been slowed (Figure 3c). More interesting is the peak between 3.5–4.0 V, which is similar for both samples during the first cycle but is much larger in the K-doped material after the 10th (Figure 3d) and 50th (Figure 3e). This is the peak associated with $Ni^{2+/4+}$, and the increase in this peak is the main reason for the increased average voltage on discharge of the K-doped material. Additionally, the high voltage discharge peak (> 4.5 V) is suppressed in both K-doped

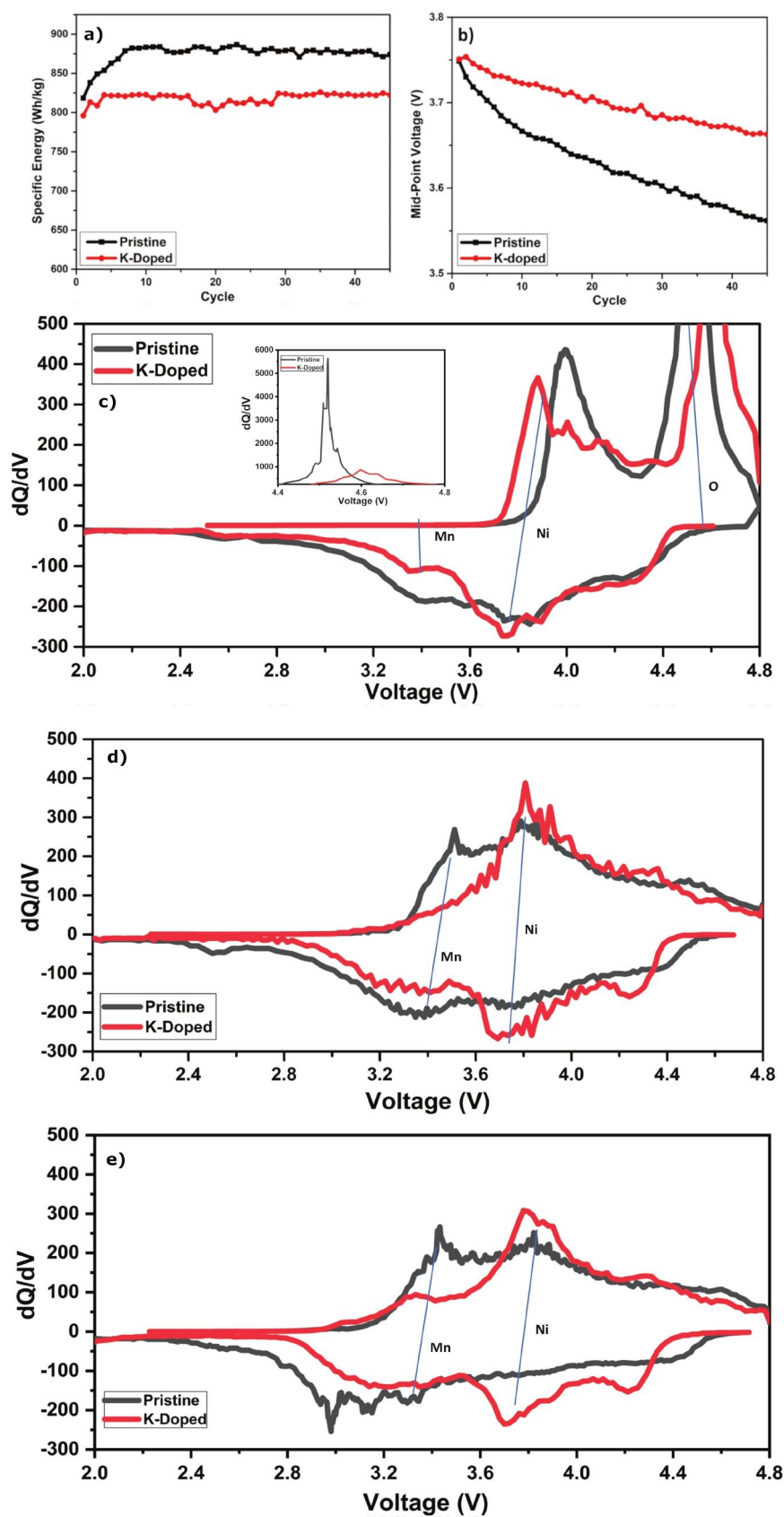


Figure 3. Electrochemical results for the Pristine and K-doped material. a) Specific Energy at 0.1 C, and b) Mid-point voltage at 0.1 C. The dQ/dV results for the d) 1st cycle (inset shows activation peak at 4.5 V), e) 10th cycle and f) 50th cycle.

materials. From this, it is possible to infer the effect of K-doping on electrochemical cycling.

The behaviour of the Ni peak suggests that the decrease in capacity is because Ni migration into the Li layer is suppressed. In the first cycle, the capacity from Ni is almost identical between the pristine and K-doped samples. This is to be expected, as capacity from Ni is independent of activation. It is only on subsequent cycles that the peak of Ni in the K-doped materials exceeds that of the pristine material. Crucially, this is because Ni peak of the pristine material decreases at a much faster rate than the Ni peak of the K-doped material. The higher voltage is therefore a result of K-doping preserving the high-voltage Ni redox throughout activation rather than by somehow increasing the amount of Ni redox. As Ni migrates into the Li layer it triggers a layered-to-spinel transition – which manifests as an increase in intensity of the low voltage region (<3.0 V) as well as a shift towards lower voltages of the pre-existing peaks – and therefore decreases the amount of high-voltage Ni redox available. Ni is the most prone to migration among all the commonly used TMs due to sharing a similar ionic radius with Li^+ .^[24] Any inhibition in TM migration is therefore manifested in Ni more strongly than the other TMs, providing strong evidence that K's effect on performance is due to its effect on Ni migration. The electrochemical results therefore demonstrate that K-doping decreases the overall capacity specifically because it decreases the amount of $\text{Mn}^{4+}/^{3+}$ redox while increasing the mid-point voltage by retaining more Ni redox during long-term cycling.

The electrochemical results provide indirect evidence that Ni migration reduces TM migration into the Li layer. In-situ XRD provides direct confirmation. Figure 4a. shows the electrochemical results of the in-situ cells, with both materials behaving similarly to the ex-situ electrochemical performance reported in Figure 1.

Figure 4b. and Figure 4c. show that there is a marked difference in the structural evolution during the first cycle between the two samples. Both samples have a relatively static structure during the initial, low-voltage (<4.0 V) region before suddenly moving significantly at ~4.1 V. This corresponds to the onset of electrochemical activity as seen in Figure 4a. The (003) peak is a direct reflection of the spacing between TM layers, while the (104) peak is a reflection of the spacing between TMs within the TM layer. Both parameters can be found in the doublet, with the (108) peak reflecting the distance between Li-layers while the (110) peak reflects the intra-layer TM spacing. A peak moving to lower angles indicates an increase in the corresponding spacing, with the opposite being true when a peak moves to higher angles. In general, as the material is charging, the inter-layer spacing increases as Li^+ is extracted and O^{2-} ions repel each other across the now vacant Li layer and the intra-layer spacing decreases and TMs are oxidised and their ionic radii decreases. As anionic redox begins at ~4.5 V, and the TMs are no longer being oxidised, then the crystal structure becomes more static in this region. During discharge the crystal structure relaxes somewhat towards its initial structure, however some permanent changes induced by activation remain. This analysis is confirmed by the Rietveld

refinement (Figure 4d). Although both materials broadly follow this trend, some profound differences can be observed when the XRD profiles are examined more closely.

The most interesting difference can be observed in the behaviour of the (108)/(110) doublet. This is an important region, because the (108) reflection at ~23.6° is associated with inter-layer spacing (similar to the (003) peak reflection), while the (110) peak is a reflection of the in-plane TM spacing.^[25,26] In the Pristine sample, both peaks behave as one would expect and move in tandem with each other. The (108) peak moves to a lower angle at the same time, and for the same reason, as the (003) peak, and the same is true of the (110) and (104) peak respectively. In the K-doped sample, however, the (108) peak remains almost completely static throughout the entire process – in stark contrast to both the pristine material and its own (110) peak, which moves to a higher angle at ~4.1 V. This common behaviour demonstrates that the oxidation of TMs, and the subsequent shrinking of their ionic radii, is a process that occurs similarly in both materials. The change in intra-layer spacing is broadly similar for both samples. However, the change in inter-layer spacing is completely different between both samples. In the pristine material – as Li^+ ions are extracted and O^{2-} ions repel each other across the now vacant Li-layer – the inter-layer spacing grows significantly before becoming static at a new, lower angle. This can be conceptualised as a transition from the initial hexagonal phase (H1) to a new hexagonal phase (H2) that is more stable at low Li^+ concentrations.^[27–29] This clear phase transition does not occur in the K-doped material. Instead, the H1 phase is maintained with an increase in the general disorder. The disorder can be explained by the low concentration of K^+ . In regions with K^+ ions they continue to screen the O^{2-} ions, meaning the lattice does not expand even as Li^+ is extracted. In regions without K^+ ions, however, this effect does not occur and so the lattice expands, resulting in significantly different inter-layer spacings in different regions and a broadening of the XRD peak. This broadening is confirmed by the Rietveld refinement (Figure 4e). More importantly, K^+ significantly inhibits the formation of H2. This has clear implications for long-term stability, but also helps explain the reduced activation.

These results suggest that K-doping is reducing activation because it is inhibiting this phase transition. The reversible TM-migration theory is therefore best able to explain these results. In the K-doped material, the TM-layer becomes more ordered as activation takes place. This is in direct contradiction to the predictions of the TM-layer nanovoids theory. The phase of the material is ultimately determined by the arrangement of the TM ions because the Li^+ ions are completely transient. Preventing the formation of H2 is therefore only possible if the movement of TM ions is significantly inhibited. The material with less TM migration therefore also has less activation, just as the reversible TM-migration theory predicts. This result mirrors similar results found in Na-ion batteries.^[30–32]

Finally, ex-situ XAS at various states of charge (SOC) was conducted to investigate any changes in oxidation caused by K-doping. XAS can be used to determine both the amount of oxidation of a particular material, as well as any change in the

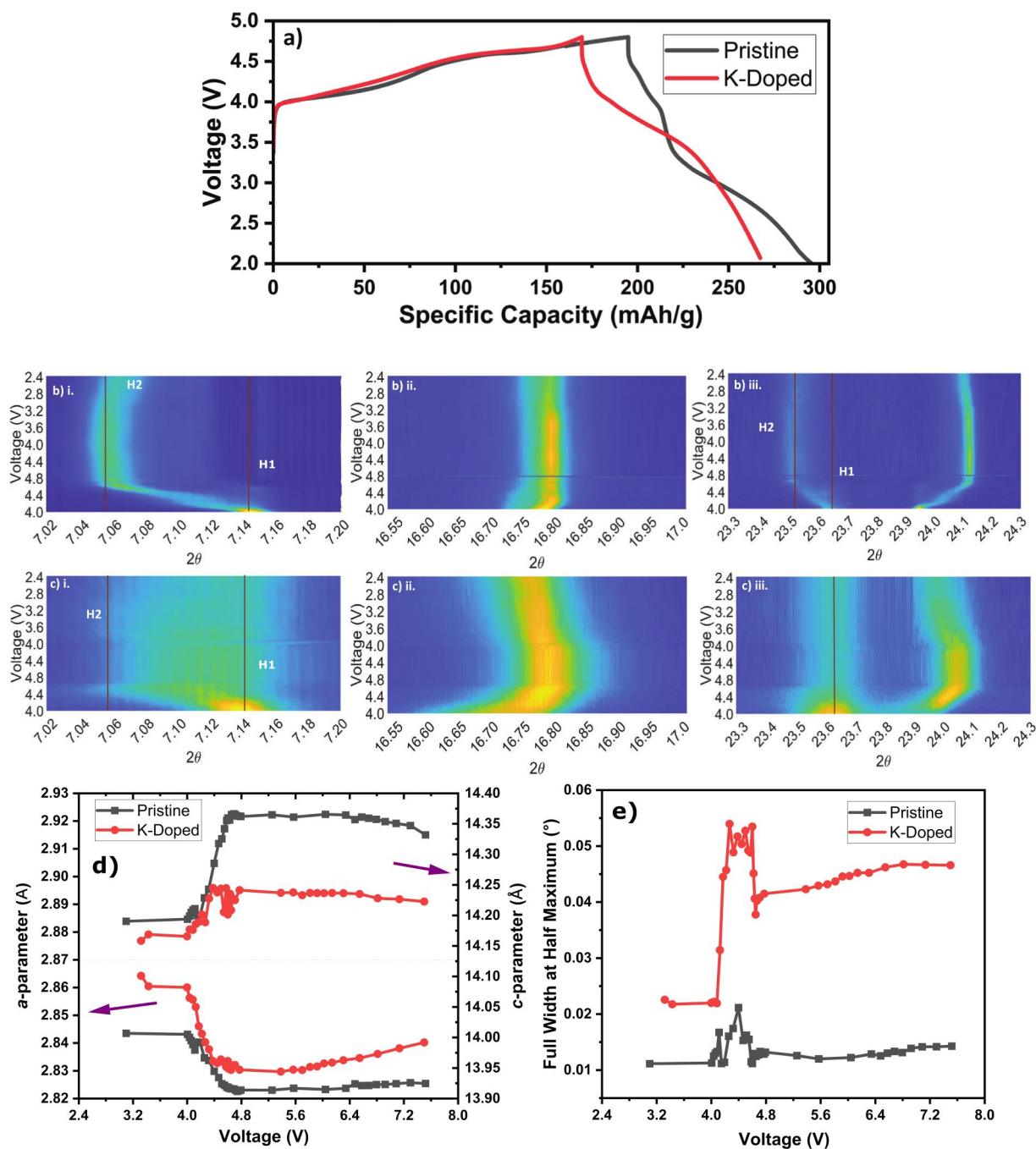


Figure 4. Results for the in-situ XRD experiment carried out at the Australian Synchrotron. **a)** Voltage vs. Capacity profile of the Pristine and K-doped sample for the first cycle. XRD results for the **b)** Pristine and **c)** K-doped sample. The (003) peak, (104) peak, and the (108)/(110) doublet, are represented by i., ii., and iii., respectively. Examples of full XRD profiles are provided in the supplementary information (Supplementary Figure 2).

energy level of the extracted electrons. In this way, XAS is able to reveal a surprising connection between Ni migration, activation, and irreversible anionic redox.

Of course, only so much information can be gleaned from analysing only the physical parameters. To gain a complete picture of activation, it is necessary to analyse the evolution of the electronic structure as well. Figure 5c shows the XAS spectra of the Ni L-edge at 4.45 V and 4.60 V for both the pristine and K-doped material and, as is consistent with previous observa-

tion, K-doping is seen to have a significant effect on Ni oxidation during the first cycle. The lower energy peak (~852.5 eV) can be assigned to Ni^{2+} , while the higher energy peak (~854.5 eV) is from Ni^{4+} .^[33] As the material is oxidised we would expect a shift towards the higher energy state, which is exactly what is observed in the K-doped material. In the pristine material, however, the opposite trend occurs, with the Ni^{2+} peak growing relative to the Ni^{4+} peak. K-doping therefore results in Ni being partially oxidised from 4.45 V to 4.60 V, in

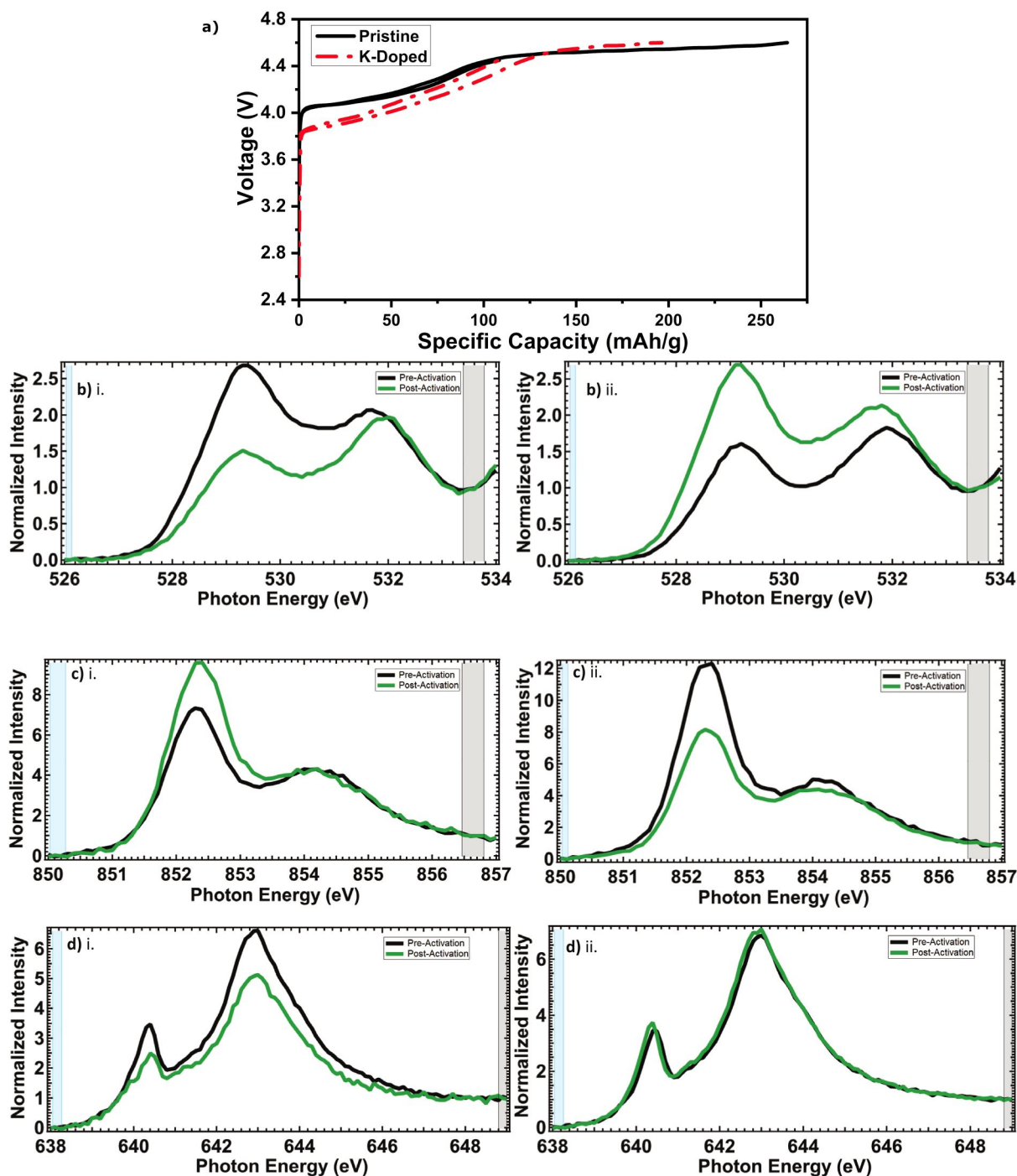


Figure 5. a) Voltage vs. Specific Capacity of the Pristine and K-doped samples. The XAS results for the b) O K-edge, c) Ni L-edge, and d) Mn L-edge are shown for the i. Pristine and ii. K-doped sample respectively.

contrast with the reduction of Ni in the pristine material. This points to a substantial difference in activation behaviour between the two samples.

The Mn L-edge results are displayed in Figure 5d and are much less conclusive. There are two Mn L-edge peaks, with the lower peak associated with Mn^{2+} while the higher energy peak is associated with $Mn^{3+/4+}$.^[34] The most important observation across both samples is that Mn is largely inactive, especially

relative to Ni and O, with the spectra hardly changing during activation. This is consistent with our dQ/dV graphs (Figure 5a) and previous reports that Mn is inactive in this voltage region, with the oxidation/reduction of Mn generally occurring at <3.6 V.^[35] TM electrochemical activity is therefore almost entirely isolated to the Ni ions during activation.

The O K-edge spectra (Figure 5b) reveals more information about the effect of K-doping on activation. Similar to the Ni L-

edge, the O K-edge displays contrasting trends for the pristine and doped material – trends which are consistent with the Ni^{4+} reduction previously observed. There are two important peaks in the O K-edge; at ~ 529.5 eV, and at ~ 531.5 eV. These can be assigned to the $\text{TM}_{3d}\text{-O}_{2p}$ antibonding orbital, and the orphaned O_{2p} orbital.^[35] As electrons are removed from an orbital, additional holes are made available for core electrons to be excited into. An increase in intensity of a peak is therefore evidence of electrons being removed from that specific orbital. As such, standard TM–O oxidation is indicated by an increase in intensity of the ~ 529.5 eV peak, while oxygen oxidation by is indicated by an increase in the ~ 531.5 eV peak. In the K-doped material, the continuing Ni oxidation results in a large increase in the TM–O peak, while a small amount of oxygen oxidation results in a correspondingly small increase in the orphaned O_{2p} peak. In the pristine material, however, a significant decrease in intensity of the TM–O peak matches the previously observed reduction of Ni. Furthermore, the higher energy O_{2p} peak is also reduced in intensity. This could be because extra electrons are being added to the O_{2p} orbitals – in other words, oxygen reduction – but the more likely explanation is that irreversible oxygen oxidation results in O_2 being lost from the lattice. Removing these oxygen molecules also removes their orbitals, therefore directly resulting in a decrease in the high energy peak's intensity. In the K-doped material we therefore have TM oxidation accompanied by a small amount of mostly reversible oxygen oxidation, while in the pristine material we can observe TM reduction coupled with a large amount of irreversible oxygen oxidation.

These results can be explained in terms of either the reversible TM migration theory or the trapped O_2 theory. Although intra-plane migration is normally invoked to explain the formation of 'voids', it is also possible for inter-plane migration to lead to the same result. Any TMs migrating into the Li layer must necessarily lead to a vacancy at the TM site. Whether the vacancy is from a migrating Li or TM is immaterial as far as activation is concerned, and so the presence of both speeds up activation. K-doping preventing TM migration therefore lessens both the number of voids created and the rate at which new voids are created on subsequent cycles, consistent with our observations. Furthermore, voids created from inter-plane TM migration are more likely to be irreversible as the TMs cannot migrate back to their original sites and remain stuck in the Li layer. K-doping increasing the apparent reversibility of oxygen oxidation is therefore also explained by reversible TM migration.

The RCM would appear to provide a solution, as the charge-transfer from ligand to metal is a crucial part of this mechanism. Li et al. observed a similar reduction of Ni after activation in their Ti-based system, which they assign to the intermediate state of a ligand-to-metal transfer.^[36] On the surface, it would appear as though these XAS results show a similar state in our Mn-based system. However, it is inaccurate to use the same mechanism to explain the results here. In Li et al.'s data, the reduction of Ni is accompanied by an increase in the 532 eV O K-edge peak just as one would expect if electrons are moving from the orphaned O 2p orbitals in the O ligands to Ni.^[35] In our

results, however, Ni reduction is accompanied by a large decrease in the 532 eV O K-edge peak. These O K-edge results show that oxygen is being irreversibly removed from the lattice in large quantities in the pristine material. Our observed reduction of Ni is therefore likely a result of electron transfer from irreversible oxygen oxidation rather than being an intermediate stage of reversible oxygen oxidation. Furthermore, the behaviour of the K-doped sample does not align with this explanation. The O K-edge results for this sample show that the O 2p states are being depopulated without large amounts of oxygen loss. In other words, oxygen oxidation is predominantly reversible in the K-doped sample. The RCM would then predict that this reversible oxygen oxidation should be accompanied by a corresponding Ni reduction. Instead, no Ni reduction is observed, with the 852 eV peak shrinking in intensity in direct contrast to the undoped sample. Ligand-to-metal transfer therefore does not cleanly explain the activation behaviour.

The activation mechanism of LRCs remains both critically important and mysterious, and by K-doping Co-free LRCs we have helped further our understanding of activation. The K-doped sample has a lower initial capacity but better stability than the pristine material. In-situ XRD demonstrates that K-doping lowers the rate of structural change in the material. Additionally, ex-situ XAS demonstrates that the pristine material undergoes significant Ni reduction and irreversible oxygen oxidation on charge, effects which are mitigated in the K-doped material. This is likely because K-doping is inhibiting TM migration and therefore limiting activation from this mechanism. The beginning of activation is described by the RCM, with this activation triggering TM migration that in turn creates additional activation. K-doping intervenes by limiting the TM migration, delaying activation and resulting in the signatures of the RCM being preserved. Understanding that activation must be conceptualised as an interaction between two distinct mechanisms opens up new avenues for practical and scientific exploration. This result provides important nuance to the existing theories of activation, and suggests that the relationship between activation and TM dynamics is even more complicated than previously thought. Particularly, these results suggest that TM reduction is critical to irreversible oxygen oxidation, and that preventing TM reduction is important – and maybe even essential – to facilitating reversible oxygen oxidation. This is an intuitive concept, as every oxidation reaction requires a corresponding reduction reaction. In an ideally functioning battery, these are separated and occur apart from one another at the cathode and anode. When O_2 is lost, there is no opportunity for the reduction reaction to take place during discharge, and so it follows that it must take place in the cathode during charge.

First-principles calculations provide insight into the potential mechanism. K remains in the Li layer during activation, and this occupation could alter the electronic state of the material. Figure 6a and Figure 6b presents the DOS results for the Mn d-orbitals and O 2p orbitals with no Li^+ , 1 Li^+ , and 1 K^+ , in the Li layer respectively. These results show that there is very little change between the three different configurations, meaning that a change in electronic structure does not explain these results. This is surprising, as one might expect such a significant difference in redox behaviour to be accompanied by a

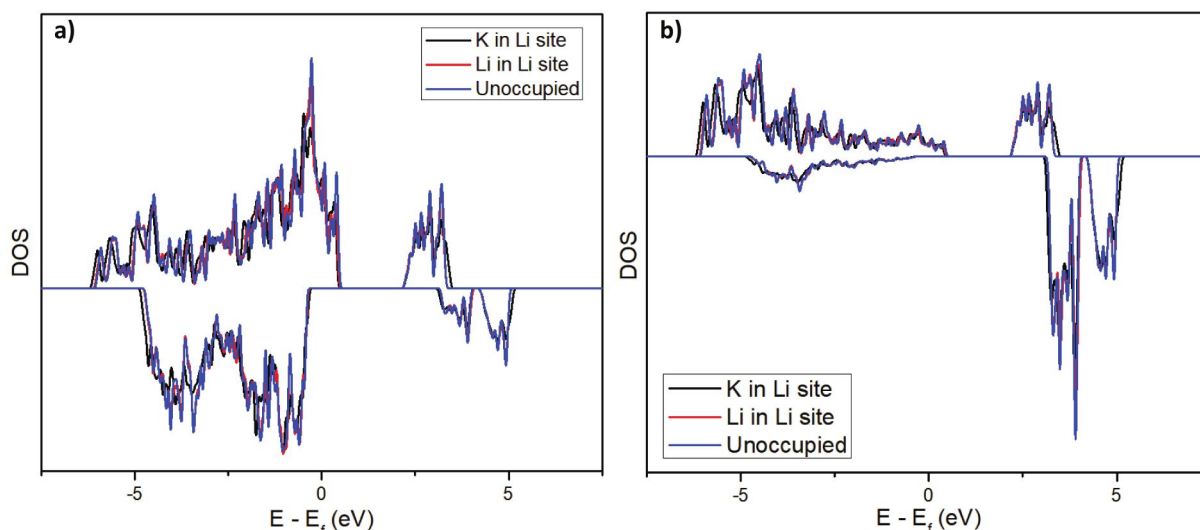


Figure 6. a) DOS results for Oxygen and b) pDOS results for Mn with different occupancy in the Li layer.

noticeable change in electronic structure. However, K has no available d orbitals which could interact with Mn or O. The steric effect of K is therefore all that remains, and this unsurprisingly has very little effect on the electronic states. This is in stark contrast to when Ni or Mn occupies those sites, which have been shown to dramatically increase the higher energy orbitals.^[2,37] This electronic reshuffling is credited with allowing oxygen redox to be semi-reversible, however K occupying the Li site and preventing TM migration means that no such reshuffling takes place. Despite this, we observe more oxidation of oxygen and less reduction of TMs.

These findings together significantly complicate the mechanism, as they alter the relationship between structural rearrangement and oxygen oxidation. This relationship underpins the most common mechanisms for explaining activation, with the competing theories being the RCM, reversible TM migration, and TM-Layer nanovoids.^[2,38]

The RCM is based on the unique electronic structure of LRCs. Unlike a normal LIB, where each oxygen is bonded to 3 TMs, the oxygens in an LRC are only bonded to 2 TMs. As the 2s orbitals of the Li⁺ ions cannot hybridise with the 2p orbitals of the oxygens. This means that there is an 'orphaned', unhybridized 2p orbital in this structure. The energy level of this state is lower than the anti-bonding TM electrons but higher than the bonding TM electrons.^[39,40] This means that, once the TM oxidation has finished, electrons can then be removed from the orphaned O 2p orbitals. According to the RCM, if the metal anti-bonding states and the O 2p states overlap, then charge can be transferred from the oxygen to the TM to stabilise the whole structure.^[4,41] Oxygen oxidation is therefore stabilised by TM reduction in this regime. If, however, the orbitals do not overlap, then the criteria for stability are different. In this regime, oxygen redox is stable if the anti-bonding oxygen orbitals are lower in energy than the TM–O hybridised orbitals. This prevents extra electrons being extracted once an (O₂)^{•-} system has formed, stabilising the material with a peroxo-like

intermediate.^[42,43] Under this theory, the reversibility and quantity of anionic redox is entirely governed by the static electronic structure during activation.^[44,45]

The activation mechanism of LRCs remains both critically important and mysterious, and by K-doping Co-free LRCs we have helped further our understanding of activation. The K-doped sample has a lower initial capacity but better stability than the pristine material. In-situ XRD demonstrates that K-doping lowers the rate of structural change in the material. Additionally, ex-situ XAS demonstrates that the pristine material undergoes significant Ni reduction and irreversible oxygen oxidation on charge, effects which are mitigated in the K-doped material. This is likely because K-doping is inhibiting TM migration and therefore limiting activation from this mechanism. The beginning of activation is described by the RCM, with this activation triggering TM migration that in turn creates additional activation. K-doping intervenes by limiting the TM migration, delaying activation and resulting in the signatures of the RCM being preserved. Understanding that activation must be conceptualised as an interaction between two distinct mechanisms opens up new avenues for practical and scientific exploration. The Reversible TM migration theory proposes that oxygen redox is stabilised by movement of TMs from the TM layer into the Li layer during charge. This changes the structure of TM–O bonds such that the unhybridized, orphaned O 2p orbital overlaps with the TM 3d orbitals. This stabilises the O₂²⁻ dimers that would otherwise oxidise to molecular O₂ and be lost.^[2,46] If this theory is correct, the reversibility of TM migration is therefore directly correlated with anionic redox reversibility. The TM-layer nanovoids theory posits that dimers are inherently unstable and will inevitably form molecular O₂. Reversibility is achieved by trapping O₂ in 'nanovoids' that form during activation. As Li⁺ is extracted from the TM layer, the vacant Li sites left behind can join together to form 'nanovoids'. Oxygen ions can then bond with each other across these nanovoids, oxidising the ions while trapping them in the lattice.^[38,47,48] Migration of TMs to form these nanovoids is therefore crucial for anionic redox in this theory, with

in-plane TM migration being favoured over out-of-plane migration. In both cases, movement of the TM ions is essential for activation and reversibility.

The activation mechanism of LRCs remains both critically important and mysterious, and by K-doping Co-free LRCs we have helped further our understanding of activation. The K-doped sample has a lower initial capacity but better stability than the pristine material. In-situ XRD demonstrates that K-doping lowers the rate of structural change in the material. Additionally, ex-situ XAS demonstrates that the pristine material undergoes significant Ni reduction and irreversible oxygen oxidation on charge, effects which are mitigated in the K-doped material. This is likely because K-doping is inhibiting TM migration and therefore limiting activation from this mechanism. The beginning of activation is described by the RCM, with this activation triggering TM migration that in turn creates additional activation. K-doping intervenes by limiting the TM migration, delaying activation and resulting in the signatures of the RCM being preserved. Understanding that activation must be conceptualised as an interaction between two distinct mechanisms opens up new avenues for practical and scientific exploration. According to this theory, the alteration of electronic states through TM migration is required for reversible oxygen redox. However, with these materials, we have shown that oxygen redox can increase while the alterations to the electronic states decreases. This supports the 'nanovoids' theory, however, as was previously explained, the in-situ XRD results (Figure 4) contradict this theory (XRD). Fortunately, the formation of nanovoids is not strictly necessary for oxygen oxidation to proceed with a similar mechanism. Under this theory, oxygen oxidation is reversible when O₂ remains trapped in the lattice and therefore is accessible on discharge. Nanovoids are simply the mechanism which allows O₂ to be trapped, and if O₂ was trapped in a similar way but without the formation of these voids then the reaction would still proceed. Just as K prevents TM migration and Li diffusion, it may also prevent diffusion of O₂ from the bulk to the surface and therefore improve activation.

O₂ can easily escape from the surface of the material, but escaping from the bulk is obviously more difficult. The movement of oxygen ions is often conceptualised in terms of the movement of oxygen vacancies rather than of oxygens themselves. Once O₂ is released from the surface, the vacancies left behind then move towards the bulk. Of course, a vacancy moving towards the centre requires an oxygen to move towards the surface, and so oxygen vacancy migration and oxygen diffusion are one and the same. Limiting the oxygen vacancy diffusion can be achieved in two ways, by 1. limiting the number of oxygen vacancies formed, and/or by 2. slowing the rate at which they propagate into the bulk. The formation energy of oxygen vacancies is strongly correlated with the number of Li vacancies, with a sharp decrease in formation energy as more Li is removed.^[49,50] By remaining in the Li layer during activation, K therefore reduces the number of vacancies which form and so slows the rate at which they penetrate the bulk. Mn migration from the TM layer to the Li layer has also been shown to dramatically reduce the energy barrier for oxygen vacancy migration.^[51] By preventing Mn migration from occurring, K doping also slows down the rate at which

vacancies diffuse. The dynamics of oxygen vacancy diffusion are therefore also an important component of activation.

The activation mechanism of LRCs remains both critically important and mysterious, and by K-doping Co-free LRCs we have helped further our understanding of activation. The K-doped sample has a lower initial capacity but better stability than the pristine material. In-situ XRD demonstrates that K-doping lowers the rate of structural change in the material. Additionally, ex-situ XAS demonstrates that the pristine material undergoes significant Ni reduction and irreversible oxygen oxidation on charge, effects which are mitigated in the K-doped material. This is likely because K-doping is inhibiting TM migration and therefore limiting activation from this mechanism. The beginning of activation is described by the RCM, with this activation triggering TM migration that in turn creates additional activation. K-doping intervenes by limiting the TM migration, delaying activation and resulting in the signatures of the RCM being preserved. Understanding that activation must be conceptualised as an interaction between two distinct mechanisms opens up new avenues for practical and scientific exploration. Overall, these results show that none out of the TM-layer nanovoids theory, reversible TM migration theory, or the RCM, can adequately explain the results of our K-doped sample in isolation. The in-situ XRD results show that K-doping inhibits the formation of the H₂ phase during activation. Meanwhile, the ex-situ XAS Ni L-edge results show that Ni is reduced in the pristine sample but oxidised in the K-doped sample. Simultaneously, the O K-edge results demonstrate irreversible oxygen loss in the pristine sample while the signature of reversible anionic redox appears in the K-doped sample. This is in direct contradiction to the RCM. One mechanism alone is therefore insufficient to completely explain the activation of our materials.

The activation mechanism of LRCs remains both critically important and mysterious, and by K-doping Co-free LRCs we have helped further our understanding of activation. The K-doped sample has a lower initial capacity but better stability than the pristine material. In-situ XRD demonstrates that K-doping lowers the rate of structural change in the material. Additionally, ex-situ XAS demonstrates that the pristine material undergoes significant Ni reduction and irreversible oxygen oxidation on charge, effects which are mitigated in the K-doped material. This is likely because K-doping is inhibiting TM migration and therefore limiting activation from this mechanism. The beginning of activation is described by the RCM, with this activation triggering TM migration that in turn creates additional activation. K-doping intervenes by limiting the TM migration, delaying activation and resulting in the signatures of the RCM being preserved. Understanding that activation must be conceptualised as an interaction between two distinct mechanisms opens up new avenues for practical and scientific exploration. The solution is to consider the disparate activation mechanisms in a holistic way and account for their interactions with each other (Figure 7). This approach is much more powerful than considering either mechanism alone, and is able to unravel the apparent contradictions in our results. During the initial activation, before any large-scale TM migration has taken place, activation proceeds according to the RCM. While this is a largely reversible process, some irreversibility is inevitable and therefore so is the generation of some oxygen vacancies. These

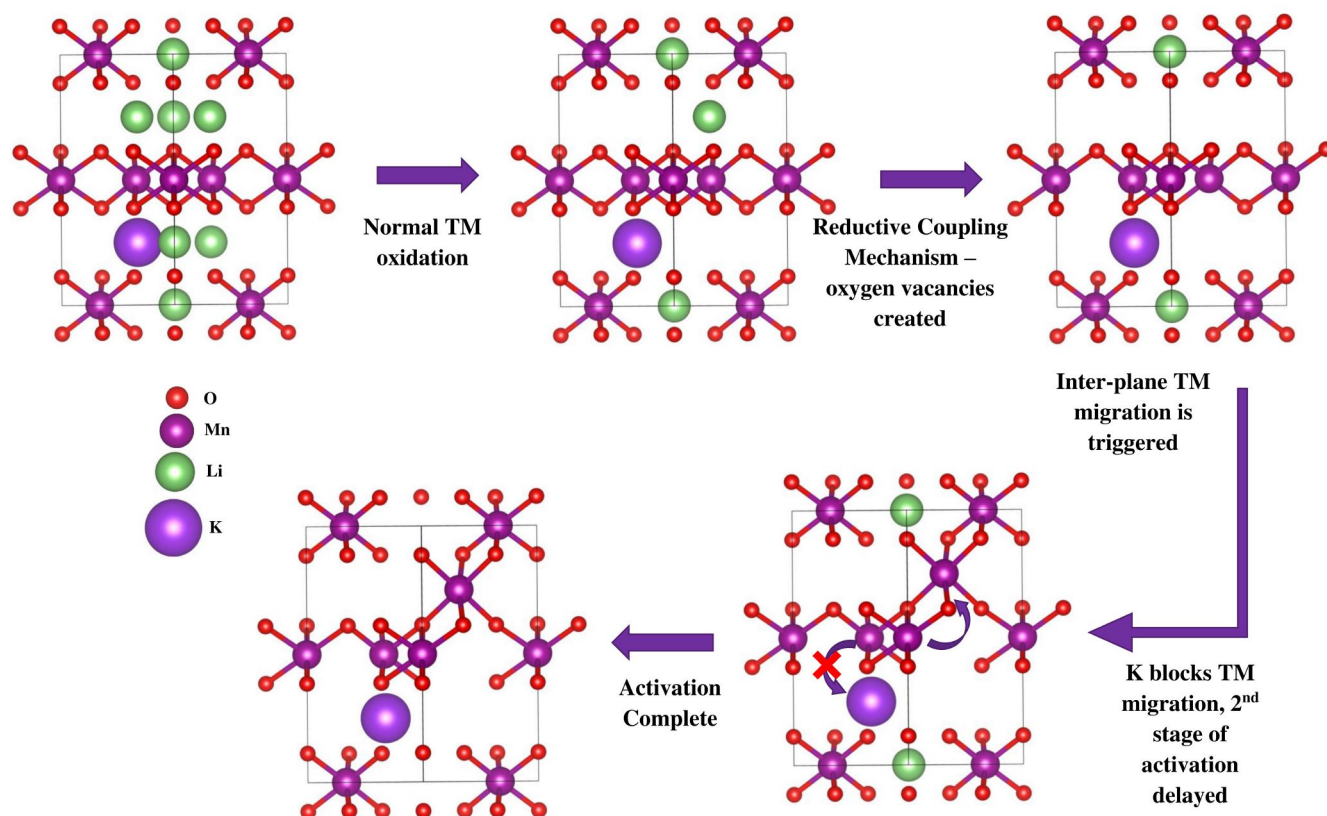


Figure 7. Schematic of the proposed activation mechanism. K does not affect the RCM stage of activation, but interrupts the inter-plane TM migration stage.^[52]

oxygen vacancies act as a trigger for TM migration, as they significantly lower the energy barrier for TM migration. This is reflected in the in-situ XRD data. The crystal structure remains static at low voltages before a sudden and drastic movement during activation. The TM migration then triggers additional activation according to the reversible TM migration mechanism, which in turn generates additional small irreversibilities and therefore more TM migration in a limited feedback loop. In the pristine material there is nothing to stop this process, resulting in faster activation and greater capacity during the first cycle. This faster activation, however, comes at the cost of more irreversibility. This can be seen in the XAS results, with the combination of the Ni L-edge and O K-edge providing strong evidence for irreversible anionic redox. In the K-doped sample, however, the potassium ions physically block TM migration as evidenced by Figure 4b. This inhibits the activation during the TM migration phase and limits the effect of the feedback loop. Activation in the K-doped sample is therefore much slower than in the pristine sample, reflected in both the lower initial capacity and the steady increase in capacity over dozens of cycles. This is also reflected in the O K-edge, with the signature peak at ~531 eV being preserved in the K-doped sample because the second stage of activation has been so inhibited. K-doping therefore slows down activation from TM migration – by blocking TM movements – while preserving activation from the RCM by maintaining the electronic structure of the pristine sample.

This has important implications, both for K-doping in specific and LRCs as a whole. Firstly, it suggests that the effect of K-doping on activation is an important reason for its improvement in stability. By delaying activation and preventing the ‘feedback loop’ from getting started it increases the reversibility of activation and therefore maintains its capacity for many more cycles. Secondly, it suggests that activation should be analysed as a holistic combination of the RCM and the reversible TM migration mechanism rather than as either alone. Not only is this a new understanding of activation, but it allows for a more refined approach to optimising LRCs.

Conclusions

The activation mechanism of LRCs remains both critically important and mysterious, and by K-doping Co-free LRCs we have helped further our understanding of activation. The K-doped sample has a lower initial capacity but better stability than the pristine material. In-situ XRD demonstrates that K-doping lowers the rate of structural change in the material. Additionally, ex-situ XAS demonstrates that the pristine material undergoes significant Ni reduction and irreversible oxygen oxidation on charge, effects which are mitigated in the K-doped material. This is likely because K-doping is inhibiting TM migration and therefore limiting activation from this mechanism. The beginning of activation is

described by the RCM, with this activation triggering TM migration that in turn creates additional activation. K-doping intervenes by limiting the TM migration, delaying activation and resulting in the signatures of the RCM being preserved. Understanding that activation must be conceptualised as an interaction between two distinct mechanisms opens up new avenues for practical and scientific exploration.

Acknowledgements

The authors acknowledge the support from the Australian Government through the Australian Research Council's Laureate Fellowship (FL190100139) and Cooperative Research Centre Program (CRC-P). X H thanks the Queensland Government for the Queensland Advanced Science Fellowship support. We acknowledge access to computational resources at the NCI National Facility through the National Computational Merit Allocation Scheme supported by the Australian Government. We also acknowledge support from the Queensland Cyber Infrastructure Foundation (QCIF) and the University of Queensland Research Computing Center (UQ RCC). Open Access publishing facilitated by The University of Queensland, as part of the Wiley - The University of Queensland agreement via the Council of Australian University Librarians.

Conflict of Interests

The authors declare no conflict of interest.

Data Availability Statement

The data that support the findings of this study are available from the corresponding author upon reasonable request.

Keywords: Li-Rich Cathodes · Potassium Doping · Li-ion Battery · Electrochemistry

- [1] S. Hu, et al., *Electrochem. Energy Rev.* **2019**, *2*(2), 277–311.
- [2] W. E. Gent, et al., *Nat. Commun.* **2017**, *8*(1).
- [3] R. A. House, et al., *Energy Environ. Sci.* **2022**, *15*(1), 376–383.
- [4] M. Ben Yahia, et al., *Nat. Mater.* **2019**, *18*(5), 496–502.
- [5] Q. Li, et al., *ACS Appl. Mater. Interfaces* **2014**, *6*(13), 10330–10341.
- [6] Z. Liu, et al., *Solid State Ionics* **2019**, *332*, 47–54.

- [7] J. Reed, G. Ceder, A. Van Der Ven, *Electrochem. Solid-State Lett.* **2001**, *4*(6), A78.
- [8] C.-C. Wang, Y.-C. Lin, P.-H. Chou, *RSC Adv.* **2015**, *5*(84), 68919–68928.
- [9] Y. Wang, et al., *Nat. Commun.* **2021**, *12*(1), 13.
- [10] J. Zhao, et al., *Energy Technol.* **2018**, *6*(12), 2358–2366.
- [11] J. Wang, et al., *Phys. Chem. Chem. Phys.* **2019**, *21*(43), 24017–24025.
- [12] P. P. Dahiya, et al., *J. Electrochem. Soc.* **2018**, *165*(11), A2536–A2548.
- [13] C. Liu, et al., *J. Alloys Compd.* **2019**, *787*, 700–710.
- [14] T. Xu, et al., *J. Mater. Sci.* **2021**, *56*(3), 2399–2411.
- [15] A. Van Der Ven, et al., *Phys. Rev. B* **2001**, *64*(18).
- [16] Z. Zheng, et al., *Electrochim. Acta* **2016**, *188*, 336–343.
- [17] D. D. Korobov, et al., *Mater. Today: Proc.* **2020**, *30*.
- [18] G. Kresse, J. Furthmüller, *Phys. Rev. B* **1996**, *54*(16), 11169–11186.
- [19] J. P. Perdew, K. Burke, M. Ernzerhof, *Phys. Rev. Lett.* **1996**, *77*(18), 3865–3868.
- [20] S. Grimme, et al., *J. Chem. Phys.* **2010**, *132*(15).
- [21] S. Grimme, S. Ehrlich, L. Goerigk, *J. Comput. Chem.* **2011**, *32*(7), 1456–1465.
- [22] G. Pirug, A. Winkler, H. P. Bonzel, *Surf. Sci.* **1985**, *163*(1), 153–171.
- [23] G. Greczynski, L. Hultman, *Angew. Chem. Int. Ed.* **2020**, *59*(13), 5002–5006.
- [24] C.-H. Shen, et al., *ACS Appl. Mater. Interfaces* **2014**, *6*(15), 13271–13279.
- [25] C. R. Fell, et al., *Solid State Ionics* **2012**, *207*, 44–49.
- [26] T. Ohzuku, A. Ueda, M. Nagayama, *J. Electrochem. Soc.* **1993**, *140*(7), 1862.
- [27] X. Q. Yang, X. Sun, J. McBreen, *Electrochem. Commun.* **1999**, *1*(6), 227–232.
- [28] Q. Xie, W. Li, A. Manthiram, *Chem. Mater.* **2019**, *31*(3), 938–946.
- [29] S. Jamil, et al., *J. Mater. Chem. A* **2020**, *8*(40), 21306–21316.
- [30] Y. Lai, et al., *Adv. Mater.* **2022**, *34*(47), 2206039.
- [31] Y. Wang, et al., *Adv. Funct. Mater.* **2020**, *30*(13), 1910327.
- [32] L. Xiao, et al., *Small* **2023**, *19*(1), 2205732.
- [33] M. Oishi, et al., *J. Power Sources* **2013**, *222*, 45–51.
- [34] K. Kubobuchi, et al., *Appl. Phys. Lett.* **2014**, *104*(5), 053906.
- [35] M. Oishi, et al., *J. Power Sources* **2015**, *276*, 89–94.
- [36] B. Li, et al., *Nat. Mater.* **2022**, *21*(10), 1165–1174.
- [37] D. Eum, et al., *Nat. Mater.* **2022**, *21*(6), 664–672.
- [38] R. A. House, et al., *Nat. Energy* **2021**, *6*(8), 781–789.
- [39] D.-H. Seo, et al., *Nat. Chem.* **2016**, *8*(7), 692–697.
- [40] J. Zaanen, G. A. Sawatzky, J. W. Allen, *Phys. Rev. Lett.* **1985**, *55*(4), 418–421.
- [41] M. Saubanère, et al., *Energy Environ. Sci.* **2016**, *9*(3), 984–991.
- [42] K. Luo, et al., *Nat. Chem.* **2016**, *8*(7), 684–691.
- [43] K. Luo, et al., *J. Am. Chem. Soc.* **2016**, *138*(35), 11211–11218.
- [44] B. Li, et al., *Adv. Funct. Mater.* **2014**, *24*(32), 5112–5118.
- [45] M. Sathiyaraj, et al., *Nat. Mater.* **2013**, *12*(9), 827–835.
- [46] J. Hong, et al., *Nat. Mater.* **2019**, *18*(3), 256–265.
- [47] R. A. House, et al., *Nat. Energy* **2020**, *5*(10), 777–785.
- [48] R. A. House, et al., *Nature* **2020**, *577*(7791), 502–508.
- [49] W. Hu, et al., *Solid State Ionics* **2020**, *347*, 115257.
- [50] P. Yan, et al., *Nat. Nanotechnol.* **2019**, *14*(6), 602–608.
- [51] S. Lee, et al., *Angew. Chem. Int. Ed.* **2019**, *58*(31), 10478–10485.
- [52] K. Momma, F. Izumi, *J. Appl. Crystallogr.* **2011**, *44*(6), 1272–1276.

Manuscript received: February 20, 2024

Revised manuscript received: January 3, 2025

Accepted manuscript online: January 16, 2025

Version of record online: February 26, 2025